Novel Scattering Operator for Arbitrary Finite Element Models in Optical Waveguides

Novel Scattering Operator for Arbitrary Finite Element Models in Optical Waveguides

Keita Morimoto, *Student Member, IEEE*, Akito Iguchi, *Member, IEEE*, and Yasuhide Tsuji, *Senior Member, IEEE*, *Senior Member, OSA*

***Abstract*—An efficient finite-element-method-based scattering operator (FEM-SO) is proposed. Utilizing field based propagation operators as boundary conditions, arbitrary light waves including radiation and evanescent waves can be treated at input and output ports. In contrast to conventional scattering operator techniques, the FEM-SO is applicable to arbitrary structures by using finite element models. In addition, considering structural discontinuities at the connecting boundary of scattering operators, an interface matrix to satisfy the boundary conditions between unit structures is introduced. To verify the present approach, numerical examples are shown for propagation characteristics of high-index-contrast waveguide facet and power spectrum of a photonic-crystal Fabry-Pérot (FP) cavity filter.**

***Index Terms*—Scattering operators, finite element method (FEM), propagation operator, boundary conditions, waveguide discontinuities.**

I. Introduction

In order to design high performance photonic devices that are fundamental components of optical communication systems and integrated optical circuits, a highly efficient and flexible numerical analysis method has been required. Beam propagation method (BPM) is well known as a high efficient technique for study of light propagation in longitudinally varying optical structures [1]–[6]. However, the BPM only deals with the forward propagating optical field, and thus, they are useful only if the structure has small refractive index contrast or sufficiently slowly-varying refractive index along the propagation direction. For accurate modeling in many practical optical devices with refractive index discontinuities along the propagation direction, another approach considering interaction of forward and backward waves is needed.

Transfer matrix methods (TMM) [7]–[14] and scattering operator (SO) techniques [15]–[20] are effective approaches to analyze waveguide structures involving multiple dielectric interfaces while reducing unnecessary computation in each invariant segment along the propagation direction. The TMM and SO are formulated by boundary conditions at the discontinuity facets and eigenfields in each segment. Mode-based approach which is so called bidirectional eigenmode propagation (BEP) [7]–[10] and field-based approach which is so called bidirectional BPM (BiBPM) [11]–[13] are introduced to construct TMM. Compared between these approaches, the field-based approach is suitable for open system problems because it can deal with not only guided modes but also radiation modes. On the other hand, it has been reported that TMM often suffers from numerical instability, and SO techniques based on BEP [15]–[17] and BiBPM [18]–[20] have been studied as relatively stable schemes. In an optimal design process of optical devices, these analysis methods can improve the computational efficiency by not only reducing a number of discretization but also recalculating only the matrix related to structural variation. However, since each segment needs to be a uniform structure in propagation direction, design freedom is greatly restricted. Especially in recent topology optimization designs [21]–[23], more rigorous analysis for arbitrary structures is required due to generation of complicated structures, that lies outside the scope of conventional TMM and SO. In [14], we have presented a TMM which combines a conventional BPM and field-based propagation operator method (POM) so that the segments whose structure varies in the propagation direction can be considered. Although the propagation operator technique has high accuracy in waveguide discontinuity problems [24]–[26], the propagation angle of the TMM is still constrained because of limitation of slowly varying envelope approximation. Therefore, direct discretization approaches such as finite element method (FEM) are still essential [27], [28]. Unlike TMM and SO techniques, the conventional FEM has to solve large-scale simultaneous linear equations in every time the structure is updated in a design process, that leads large computational cost.

In this paper, we first present a numerical technique using FEM based SO (FEM-SO) for analysis of optical waveguides with arbitrary finite element models in multiple stages. In the analysis of microwave circuits, mode-based scattering matrices are often used for efficient analysis to divide large-scale circuits into basic elements. However, in the analysis of open systems like optical circuits, mode-based approach is not always suitable because radiated waves may couple with guided modes of latter stage elements. Thus, field-based SO based on finite element models is crucial and suitable for the analysis of open systems. For this purpose, boundary condition based on the POM is applied to the input and output ports to allow propagation of arbitrary field at the connecting interface. While brief explanation of how converting simultaneous linear equations of the FEM into a scattering matrix is shown in our recent report [29], a connectivity of the scattering matrix has not been studied. In addition, we introduce an interface matrix that satisfies the boundary conditions at discontinuous connect-

Manuscript received September 14, 2020; revised January 6, 2021; accepted February 16, 2021. This work was supported by JSPS KAKENHI under Grant 18K04276. *(Corresponding author: Yasuhide Tsuji; Keita Morimoto.)*
K. Morimoto, A. Iguchi and Y. Tsuji are with the Division of Information and Electronic Engineering, Muroran Institute of Technology, Muroran, 050-8585 Japan (e-mail: 19096015@mmm.muroran-it.ac.jp; iguchia@mmm.muroran-it.ac.jp; y-tsuji@mmm.muroran-it.ac.jp).

ing interface. To verify the present approach, numerical examples for propagation characteristics of high-index-contrast waveguide facet and power spectrum of a photonic-crystal Fabry-Pérot (FP) cavity filter are demonstrated. The proposed method can be applied to various optical device designs and will be a good candidate to overcome the computational cost problem by eliminating unnecessary recalculations of large-scale simultaneous linear equations during optimal design. Domain decomposition method (DDM), which is a popular technique for allowing parallel computation [30], [31], usually divides whole analysis region into multiple subdomains and fields at interfaces are self-consistently determined by iterative calculation. On the other hand, our FEM-SO approach does not require recalculation of simultaneous linear equation once scattering operator is derived. Thus, when arbitrary different incidence field is given to the same system, its response can be efficiently calculated by just calculating a matrix and vector product. In addition, our approach is suitable to an optimal design because the scattering operator of the entire structure can be readily reconstructed with a lower computational cost when a part of the entire structure is modified during an optimal design.

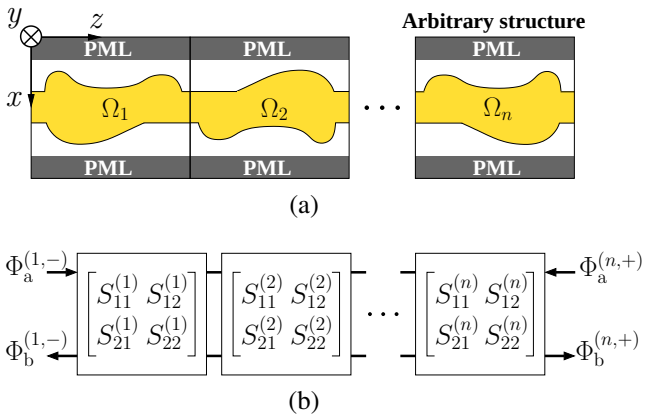

Fig. 1. Connection of arbitrary waveguide structures: (a) schematic of the waveguide geometry; (b) scattering matrix representation.

II. FORMULATIONS

A. Finite Element Discretization

We consider a two-dimensional (2-D) optical waveguide with implementation of perfectly matched layers (PMLs) as shown in Fig. 1(a), where the computational window is in the xz plane and there is no variation along the y direction ($\partial/\partial y = 0$). The unit segment Ω_i $(i = 1, 2, \cdots, n)$ has two interfaces at distinct locations in the propagation direction for connecting to adjacent structures, i.e. Ω_{i-1} and Ω_{i+1}. Considering Maxwell's equations with PML, we obtain the following basic equation:

$$\frac{\partial}{\partial x}\left(\frac{p}{s_x}\frac{\partial \Phi}{\partial x}\right) + s_x \frac{\partial}{\partial z}\left(p\frac{\partial \Phi}{\partial z}\right) + k_0^2 q s_x \Phi = 0 \qquad (1)$$

where k_0 is the free space wavenumber, $\Phi = \sqrt{\varepsilon_0}E_y$, $p = 1$, $q = n^2$ for TE modes, and $\Phi = \sqrt{\mu_0}H_y$, $p = 1/n^2$, $q = 1$ for TM modes. E_y and H_y are y components of electric and magnetic fields, respectively, and n is the refractive index. s_x represents the PML parameter and the value is taken as

$$s_x = \begin{cases} 1 & \text{in non-PML region} \\ 1 - j\left(\rho/d_x\right)^2 \tan\delta & \text{in PML region} \end{cases} \qquad (2)$$

where ρ is the distance from the beginning of PML and δ is the loss angle at the end of PML ($\rho = d_x$).

Dividing the analysis region into quadratic (second-order) triangular elements, and applying FEM based on Galerkin method to (1), we obtain the following linear equation in matrix form:

$$[P]\{\Phi\} = \{u\} \qquad (3)$$

$$[P] = \sum_e \iint_e \left[\frac{p}{s_x}\frac{\partial\{N\}}{\partial x}\frac{\partial\{N\}^T}{\partial x} + p s_x \frac{\partial\{N\}}{\partial z}\frac{\partial\{N\}^T}{\partial z} - k_0^2 q s_x \{N\}\{N\}^T\right] dxdz \qquad (4)$$

$$\{u\} = \sum_{\chi=-,+}\left(\sum_{e_\chi}{}' \int_{e_\chi} p s_x \{\tilde{N}\}\frac{\partial \Phi}{\partial n_z} dx\right) \qquad (5)$$

where the components of vector $\{\Phi\}$ are the values of Φ at all nodal points in the entire analysis region, $\sum_e$ extends over all the different elements, and $\sum'_{e_\chi}$ extends over the elements related to the input ($\chi = -$) and output ($\chi = +$) boundary. $\{\tilde{N}\}$ is the shape function vector for quadratic line element at two interfaces. (3) can also be written in its extended version as

$$\begin{bmatrix} [P_{00}] & [P_{0-}] & [P_{0+}] \\ [P_{-0}] & [P_{--}] & [P_{-+}] \\ [P_{+0}] & [P_{+-}] & [P_{++}] \end{bmatrix} \begin{bmatrix} \{\Phi\}_0 \\ \{\Phi\}_- \\ \{\Phi\}_+ \end{bmatrix} = \begin{bmatrix} \{0\} \\ \{u\}_- \\ \{u\}_+ \end{bmatrix} \qquad (6)$$

where $\{u\}_-$ and $\{u\}_+$ can be regarded as the boundary conditions at input and output ports, respectively. In order to construct the scattering operators from (6), the boundary conditions have to cover arbitrary electromagnetic fields. Mode expansion based boundary condition [32] is usually expensive to calculate various required modes including radiation and evanescent modes. Boundary condition based on paraxial approximation [33] and Padé approximation [34] cause deterioration of accuracy in problems with large refractive index differences. On the other hand, POM boundary condition shown in our previous work [29] has sufficient accuracy and efficiency even in the case of strongly guiding optical waveguides, and thus, we employ the POM boundary condition.

B. POM Boundary Condition

In the POM, $\{\Phi\}_\chi$ $(\chi = -, +)$ is governed by the following equation:

$$\frac{d^2\{\Phi\}_\chi}{dn_z^2} + [Q]_\chi^2\{\Phi\}_\chi = \{0\} \tag{7}$$

where d/dn_z represents the partial derivative along the outward z direction, $\{0\}$ is the null vector, and $[Q]_\chi$ is the characteristic matrix of each boundary written by

$$[Q]_\chi^2 = [M]_\chi^{-1}[K]_\chi \tag{8}$$

$$[M]_\chi = \sum_{e_\chi}{}' \int_{e_\chi} p s_x \{\tilde{N}\}_\chi \{\tilde{N}\}_\chi^T dx \tag{9}$$

$$[K]_\chi = \sum_{e_\chi}{}' \int_{e_\chi} \left[k_0^2 q s_x \{\tilde{N}\}_\chi \{\tilde{N}\}_\chi^T - \frac{p}{s_x}\frac{d\{\tilde{N}\}_\chi}{dx}\frac{d\{\tilde{N}\}_\chi^T}{dx} \right] dx \tag{10}$$

where $[M]_\chi$ and $[K]_\chi$ is a finite element mass matrix and stiffness matrix, respectively, for eigenmode analysis on each boundary. As a solution of the differential equation (7), $\{\Phi\}_\chi$ can be formally expressed as

$$\begin{aligned}\{\Phi\}_\chi &= \{\Phi_a^{(\chi)}\} + \{\Phi_b^{(\chi)}\} \\ &= \exp(j[Q]_\chi n_z)\{\phi_{\mathrm{a}}^{(\chi)}\} + \exp(-j[Q]_\chi n_z)\{\phi_{\mathrm{b}}^{(\chi)}\}\end{aligned} \tag{11}$$

where $\{\phi_{\mathrm{a}}\}_\chi$ and $\{\phi_{\mathrm{b}}\}_\chi$ represent vectors standing for inward and outward propagation fields, respectively, under the condition that the outward normal direction of the boundary is positive. Differentiating (11) and eliminating $\{\Phi_{\mathrm{b}}^{(\chi)}\}$, we obtain

$$\frac{d\{\Phi\}_\chi}{dn_z} = j2[Q]_\chi\{\Phi_a^{(\chi)}\} - j[Q]_\chi\{\Phi\}_\chi. \tag{12}$$

$\{u\}$ can be rewritten by utilizing (9) and (12), and thus, we obtain the following equation:

$$\begin{bmatrix} [P_{00}] & [P_{0-}] & [P_{0+}] \\ [P_{-0}] & [\tilde{P}_{--}] & [P_{-+}] \\ [P_{+0}] & [P_{+-}] & [\tilde{P}_{++}] \end{bmatrix} \begin{bmatrix} \{\Phi\}_0 \\ \{\Phi\}_- \\ \{\Phi\}_+ \end{bmatrix} = \begin{bmatrix} \{0\} \\ 2[C]_-\{\Phi_{\mathrm{a}}^{(-)}\} \\ 2[C]_+\{\Phi_{\mathrm{a}}^{(+)}\} \end{bmatrix} \tag{13}$$

with

$$[\tilde{P}_{\chi\chi}] = [P_{\chi\chi}] + [C]_\chi \tag{14}$$

$$[C]_\chi = j[M]_\chi[Q]_\chi \qquad \text{for } \chi = - \text{ or } +. \tag{15}$$

$[Q]_\chi$ is defined as the square root matrix of (8). This matrix is approximated by Denman-Beavers iterative (DBI) scheme with a branch-cut rotation in the complex plane whose accuracy and stability are reported to be higher than those of Padé approximation [25], [26].

C. Construction of Scattering Matrix

Since SO techniques are aimed at obtaining the input-output response, the internal electromagnetic fields $\{\Phi\}_0$ virtually is not required. Eliminating $\{\Phi\}_0$ from (13) , we obtain the scattering matrix in certain segment Ω_i as below:

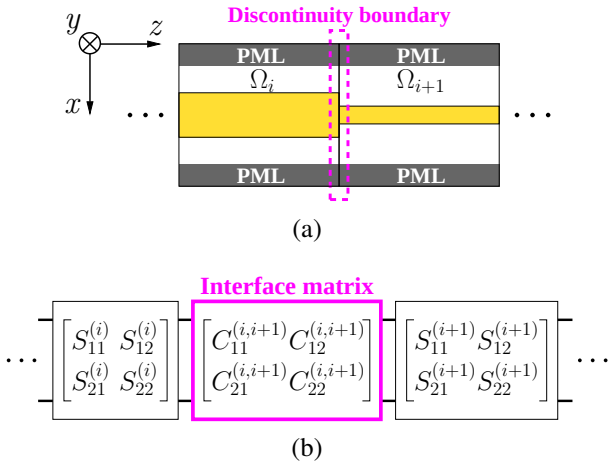

Fig. 2. Waveguide discontinuity: (a) schematic of the waveguide geometry; (b) scattering matrix representation.

$$\begin{bmatrix} \{\Phi_{\mathrm{b}}^{(i,-)}\} \\ \{\Phi_{\mathrm{b}}^{(i,+)}\} \end{bmatrix} = \begin{bmatrix} [S]_{11}^{(i)} & [S]_{12}^{(i)} \\ [S]_{21}^{(i)} & [S]_{22}^{(i)} \end{bmatrix} \begin{bmatrix} \{\Phi_{\mathrm{a}}^{(i,-)}\} \\ \{\Phi_{\mathrm{a}}^{(i,+)}\} \end{bmatrix} \tag{16}$$

with

$$[S]_{11}^{(i)} = 2[T]_1^{-1}[C]_- - [I] \tag{17}$$

$$[S]_{12}^{(i)} = 2[U]_1[T]_2^{-1}[C]_+ \tag{18}$$

$$[S]_{21}^{(i)} = 2[U]_2[T]_1^{-1}[C]_- \tag{19}$$

$$[S]_{22}^{(i)} = 2[T]_2^{-1}[C]_+ - [I] \tag{20}$$

$$[T]_1 = [\tilde{P}_{--}] - [P_{-0}][P_{00}]^{-1}([P_{0-}] + [P_{0+}][U]_+) \tag{21}$$

$$[T]_2 = [\tilde{P}_{++}] - [P_{+0}][P_{00}]^{-1}([P_{0+}] + [P_{0-}][U]_-) \tag{22}$$

$$[U]_1 = ([\tilde{P}_{--}] - [P_{-0}][P_{00}]^{-1}[P_{0-}])^{-1}[P_{-0}][P_{00}]^{-1}[P_{0+}] \tag{23}$$

$$[U]_2 = ([\tilde{P}_{++}] - [P_{+0}][P_{00}]^{-1}[P_{0+}])^{-1}[P_{+0}][P_{00}]^{-1}[P_{0-}] \tag{24}$$

where $[I]$ is an identity matrix, $[S]_{mn}^{(i)}$ $(m, n = 1, 2)$ is a scattering operator. We note that these expressions are derived under a condition that elements related to input ports and output ports are independent of each other, i.e. $[P_{-+}] = [0]$ and $[P_{+-}] = [0]$. Since $[T]_i (i = 1, 2)$ is a small-scale square matrix whose size is determined by a number of nodes on each port, its inverse matrix calculation slightly contributes to increasing the total computational time. Although $[P_{00}]$ is a relatively large-scale square matrix whose size is determined by number of inner nodes, since a sparse solver can be used, its inverse matrix can be efficiently solved in the same manner as FEM calculation. Considering that an incidence from negative direction side of the z-axis, the input-output response is indicated as

$$\{\Phi_{\mathrm{b}}^{(i,+)}\} = [S]_{21}^{(i)}\{\Phi_{\mathrm{a}}^{(i,-)}\} \tag{25}$$

$$\{\Phi_{\mathrm{b}}^{(i,-)}\} = [S]_{11}^{(i)}\{\Phi_{\mathrm{a}}^{(i,-)}\}. \tag{26}$$

D. Cascading of Scattering Matrix

The constructed scattering matrix for each segment is cascaded with the adjacent segment as shown in Fig. 1(b). Here, we employ Redheffer's star product [35] to integrate into a single operator. Considering the star product with two structures of Ω_i and Ω_{i+1}, we obtain the following relation:

$$\begin{bmatrix} \{\Phi_{\rm b}\}^{(i,-)} \\ \{\Phi_{\rm b}\}^{(i+1,+)} \end{bmatrix} = \begin{bmatrix} [S_{11}^{(i,i+1)}] & [S_{12}^{(i,i+1)}] \\ [S_{21}^{(i,i+1)}] & [S_{22}^{(i,i+1)}] \end{bmatrix} \begin{bmatrix} \{\Phi_{\rm a}\}^{(i,-)} \\ \{\Phi_{\rm a}\}^{(i+1,+)} \end{bmatrix} \tag{27}$$

with

$$[S_{11}^{(i,i+1)}] = [S_{11}^{(i)}] + [S_{12}^{(i)}] \left[[I] - [S_{11}^{(i+1)}][S_{22}^{(i)}] \right]^{-1} [S_{11}^{(i+1)}][S_{21}^{(i)}] \tag{28}$$

$$[S_{12}^{(i,i+1)}] = [S_{12}^{(i)}] \left[[I] - [S_{11}^{(i+1)}][S_{22}^{(i)}] \right]^{-1} [S_{12}^{(i+1)}] \tag{29}$$

$$[S_{21}^{(i,i+1)}] = [S_{21}^{(i+1)}] \left[[I] - [S_{22}^{(i)}][S_{11}^{(i+1)}] \right]^{-1} [S_{21}^{(i)}] \tag{30}$$

$$[S_{22}^{(i,i+1)}] = [S_{22}^{(i+1)}] + [S_{21}^{(i+1)}] \left[[I] - [S_{22}^{(i)}][S_{11}^{(i+1)}] \right]^{-1} [S_{22}^{(i)}][S_{12}^{(i+1)}]. \tag{31}$$

Although, in the above derivation of cascaded scattering matrix, the inverse matrix calculation is required, the computational cost is relatively low because the sizes of their column and row are small and just equal to the number of nodes on each port.

E. Interface Matrix for a Discontinuity Interface

The POM boundary condition makes an assumption that the structure at interface continues outside the analysis region. Thus, if the scattering matrices are cascaded at discontinuity interface, the boundary condition cannot be satisfied. Here, we introduce an interface matrix (IM) to satisfy the boundary condition. This concept is schematically represented in Fig. 2. One of the boundary condition is continuity of (11). The other is continuity of the tangential component of the electromagnetic wave other than (11), which is defined by Maxwell's equations as

$$\Psi = jrp\frac{c}{\omega}\frac{\partial \Phi}{\partial z} \tag{32}$$

where c is the velocity of light, ω is an angular frequency, $\Psi = \sqrt{\mu_0}H_x$, $r = -1$ for TE modes, and $\Psi = \sqrt{\varepsilon_0}E_x$, $r = 1$ for TM modes. Applying the Galerkin method to (32) and substituting (11), the following expression is derived:

$$\{\Psi\}_\chi = j[P]_\chi \frac{c}{\omega}\frac{d\{\Phi\}_\chi}{dz} = \frac{c}{\omega}\left[-[Z]_\chi \{\Phi_a^{(\chi)}\} + [Z]_\chi \{\Phi_b^{(\chi)}\} \right] \tag{33}$$

with

$$[P]_\chi = [M_0]_\chi^{-1}[M]_\chi \tag{34}$$

$$[M_0]_\chi = \sum_{e_\chi}{}' \int_{e_\chi} r\{\tilde{N}\}_\chi \{\tilde{N}\}_\chi^T dx \tag{35}$$

$$[Z]_\chi = [P]_\chi [Q]_\chi. \tag{36}$$

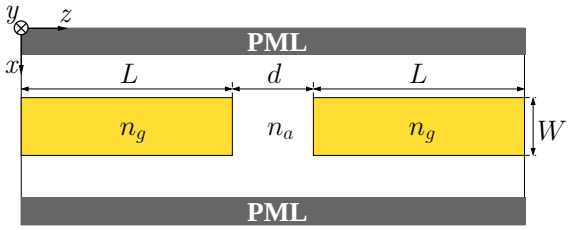

Fig. 3. Problem setup of 2-D optical waveguide with an air-gap.

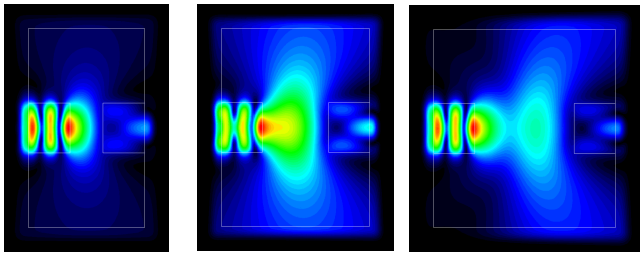

Fig. 4. Electric field distribution obtained by FEM analysis corresponding to the problem shown in Fig. 3. (a)$d = 0.4\ \mu$m, (b)$d = 0.8\ \mu$m, (c)$d = 1.2\ \mu$m.

As a result, a boundary condition between Ω_i and Ω_{i+1} can be written in matrix form as

$$\begin{bmatrix} [I] & [I] \\ [Z^{(i)}]_+ & -[Z^{(i)}]_+ \end{bmatrix} \begin{bmatrix} \{\Phi_{\rm b}^{(i,+)}\} \\ \{\Phi_{\rm a}^{(i,+)}\} \end{bmatrix} = \begin{bmatrix} [I] & [I] \\ [Z^{(i+1)}]_- & -[Z^{(i+1)}]_- \end{bmatrix} \begin{bmatrix} \{\Phi_{\rm a}^{(i+1,-)}\} \\ \{\Phi_{\rm b}^{(i+1,-)}\} \end{bmatrix}. \tag{37}$$

(37) can be easily transformed into a transfer matrix representation by taking the inverse matrix on the left-hand side, and it becomes

$$\begin{bmatrix} \{\Phi_{\rm b}\}^{(i,+)} \\ \{\Phi_{\rm a}\}^{(i,+)} \end{bmatrix} = \begin{bmatrix} [F_{11}^{(i,i+1)}] & [F_{12}^{(i,i+1)}] \\ [F_{21}^{(i,i+1)}] & [F_{22}^{(i,i+1)}] \end{bmatrix} \begin{bmatrix} \{\Phi_{\rm a}\}^{(i+1,-)} \\ \{\Phi_{\rm b}\}^{(i+1,-)} \end{bmatrix}. \tag{38}$$

In order to systematically implement our SO analysis using the above-mentioned Redheffer's star product, (38) is further transformed into a scattering matrix representation as below:

$$\begin{bmatrix} \{\Phi_{\rm a}\}^{(i,+)} \\ \{\Phi_{\rm a}\}^{(i+1,-)} \end{bmatrix} = \begin{bmatrix} [C_{11}^{(i,i+1)}] & [C_{12}^{(i,i+1)}] \\ [C_{21}^{(i,i+1)}] & [C_{22}^{(i,i+1)}] \end{bmatrix} \begin{bmatrix} \{\Phi_{\rm b}\}^{(i,+)} \\ \{\Phi_{\rm b}\}^{(i+1,-)} \end{bmatrix} \tag{39}$$

with

$$[C_{11}^{(i,i+1)}] = [F_{21}^{(i,i+1)}][F_{11}^{(i,i+1)}]^{-1} \tag{40}$$

$$[C_{12}^{(i,i+1)}] = [F_{22}^{(i,i+1)}] - [F_{21}^{(i,i+1)}][F_{11}^{(i,i+1)}]^{-1}[F_{12}^{(i,i+1)}] \tag{41}$$

$$[C_{21}^{(i,i+1)}] = [F_{11}^{(i,i+1)}]^{-1} \tag{42}$$

$$[C_{22}^{(i,i+1)}] = -[F_{11}^{(i,i+1)}]^{-1}[F_{12}^{(i,i+1)}]. \tag{43}$$

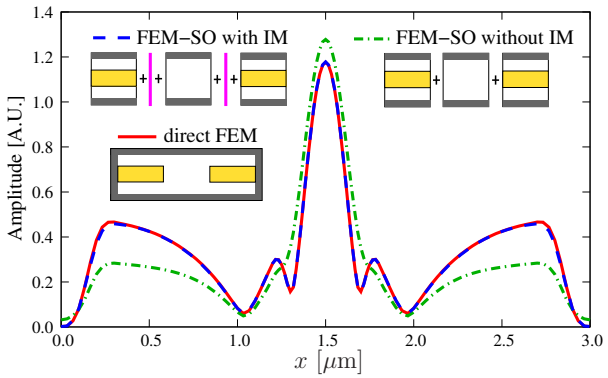

Fig. 5. Transmitted amplitude at the output port corresponding to the problem shown in Fig.3.

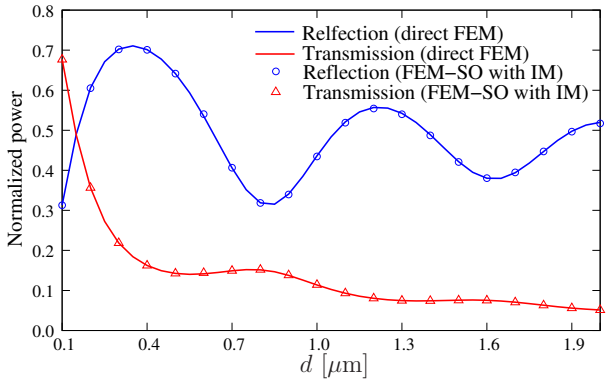

Fig. 6. Normalized reflected and transmitted power of the fundamental modes as a function of the gap length d.

III. NUMERICAL SIMULATION RESULTS

A. *Radiation from high-index-contrast waveguide facet*

First, to verify the proposed scattering operator approach, we consider the problem that an air-gap caused between high-index-contrast waveguides, and input and output waveguides are assumed to have a same structure as shown in Fig. 3. The refractive indices are $n_g = 3.6$, $n_a = 1.0$, and structural parameters are set as $W = 0.6$ μm, $L = 0.5$ μm, which supports three guided modes. Since the cladding material is assumed to be the same as that in the air-gap, many radiation and diffraction components of light are likely to occur at the waveguide facets, and thus, it requires higher accuracy than butt-joint of different waveguides with low-index-contrast. In this case, it was reported that combination method of the BPM and POM boundary condition encounters degradation of accuracy when the air-gap distance is relatively short [14]. The entire analysis region is divided into three segments which is invariant along the propagation direction. Since IM are added between adjacent segments, a total of 5 scattering matrices are connected. The necessity and validity of the IM is verified by comparing with another case where the three scattering matrices are connected without IM. In order to obtain sufficient computational accuracy, the numbers of divisions in the x and y directions are set to be 20 and 16 per 1 μm, respectively. FEM-SO has almost same computational accuracy with the conventional FEM when the same finite element mesh is used and PML region is sufficiently descritized in the conventional FEM.

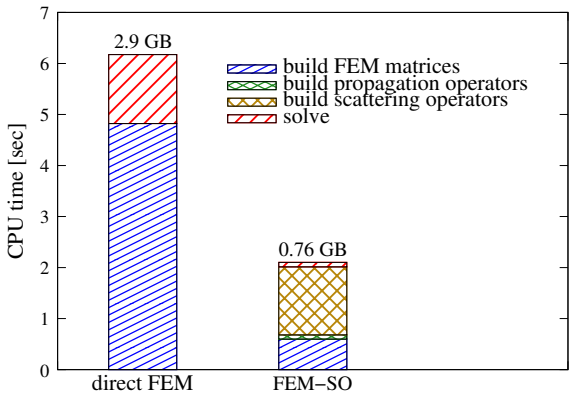

Fig. 7. CPU time and memory usage in each method for analysis of the problem shown in Fig. 3.

Figure 4 shows the electric field distributions calculated by conventional direct FEM when the air-gap distance is (a)$d = 0.4$ μm, (b)$d = 0.8$ μm, (c)$d = 1.2$ μm with respect to the incident field of fundamental TE mode and operating wavelength of $\lambda = 1.55$ μm. The computational window is 3 μm wide including PML width of 0.3 μm. In direct FEM, it is necessary to impose PML on the input and output ends to terminate the computational window, which leads to increasing of the computational cost [29]. Excitation of various radiation waves in the air-gap can be seen, and a part of them reaches the output plane. Amplitude at the output cross-sectional plane is shown in Fig. 5. While the amplitude calculated by FEM-SO with IM is in good agreement with direct FEM, FEM-SO without IM causes error of the evaluation. Practically, it is possible to avoid using IM by dividing the whole structure into substructures at continuous interface. Figure 6 shows the normalized reflected power and transmitted power of the fundamental modes as a function of the air-gap distance d. Because of Fabry-Pérot resonance and radiation loss, the reflection and transmission decrease oscillatively as d increases. From this figure, it can also be seen that the result by the FEM-SO is in good agreement with that by the direct FEM.

Figure 7 shows CPU time and memory usage in conventional direct FEM and proposed FEM-SO analysis, using Intel(R) Core(TM) i7-4770 CPU @ 3.40GHz. In the direct FEM, it takes about 6 seconds to construct the large-scale FEM matrices and solve the simultaneous linear equation. On the other hand, in the FEM-SO approach, the calculation time can be reduced to about 2 seconds because small-scale FEM matrices are constructed and only matrix product computation is required for evaluation of the wave propagation. Although, it takes the longest CPU time to make the scattering matrices in the FEM-SO, the time of making propagation operators is much shorter than the total CPU time. The computer memory used in this analysis is 0.76 GB for the FEM-SO, while it is 2.9 GB for the direct FEM.

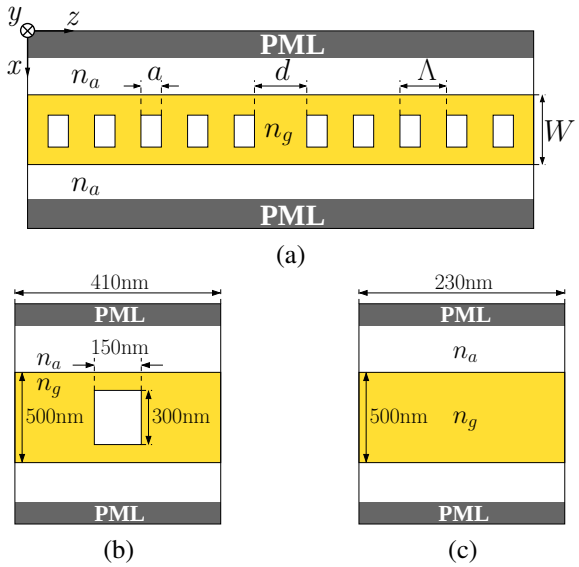

Fig. 8. Schematic arrangement of a 1-D photonic-crystal FP cavity filter:(a) is the overall structure; (b) and (c) are the unit structures which make up scattering matrices.

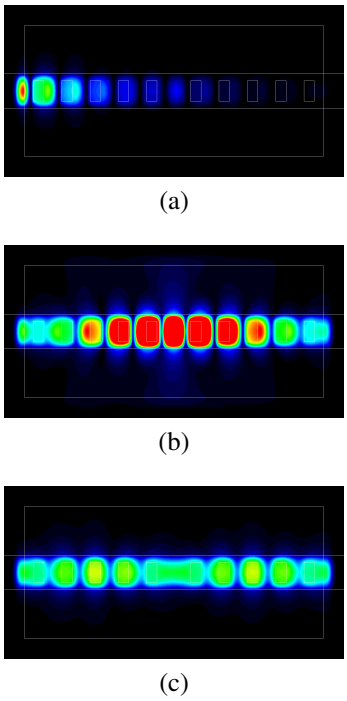

Fig. 9. Magnetic field distribution obtained by FEM analysis corresponding to the problem shown in Fig.6: (a)$\lambda = 1.55$ μm; (b)$\lambda = 1.632$ μm; (c)$\lambda = 1.85$ μm.

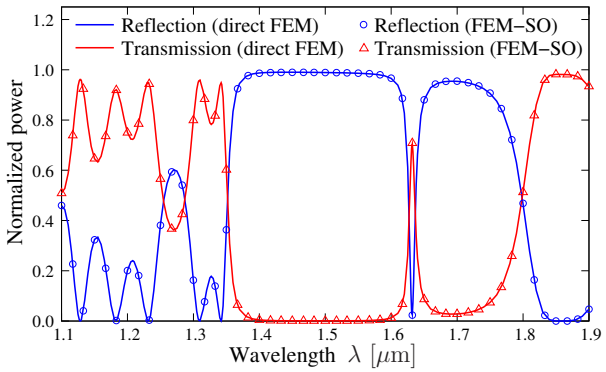

Fig. 10. Normalized reflected and transmitted power of the fundamental modes as a function of the operating wavelength λ.

B. Photonic crystal Fabry-Pérot cavity filter

Next, we show spectral transmittance and reflectance of a 1-D photonic-crystal Fabry-Pérot (FP) cavity filter in a photonic wire (see Fig. 8(a)) when the fundamental TM mode is launched. The refractive index of the wire $n_g = 2.75$ is given by an approximation of the effective refractive-index projection of a 200-nm-thick Si membrane in air, that is described in [17]. The structural parameters are set as $a = 150$ nm, $d = 490$ nm, $\Lambda = 410$ nm, $W = 500$ nm. In the case of a periodic structure, required computational resources can be significantly reduced considering only the one period. If the entire analysis region is divided at the discontinuity cross-section so that each segment has a uniform structure, it takes an additional process of generating and connecting their IM. Therefore, utilizing merit of FEM that it can discretize arbitrary structures, we divide the entire structure into fundamental segments of Fig. 8(b) and (c) with continuous interface to omit the calculation of the IM. In this example, 10 star product calculations are required in straightforward connection. For periodic structures, the computational cost can be reduced by thinking out the order of taking star products of scattering matrices. It is possible to reduce to 5 calculations of the star product in our example. In this analysis, the computational domain is divided into 7320 triangular elements to obtain sufficient computational accuracy.

In Fig. 9, magnetic field distribution in the FP cavity filter at wavelength $\lambda = 1.55$ μm, $\lambda = 1.632$ μm, and $\lambda = 1.85$ μm are shown. Due to resonance in the cavity, the power transmission is varied depending on the operating wavelength. This resonant wavelength is tuned by changing d or W. The resonant wavelength shifts to shorter wavelength side as d or W decreases. In addition, stop band also shifts to shorter wavelength side as W decreases because the phase constant decreases. The calculated spectral characteristics are shown in Fig. 10. It can be seen that the spectral characteristics obtained by the FEM-SO is in good agreement with those of the direct FEM. Figure 11 shows CPU time and memory usage in conventional direct FEM and proposed FEM-SO analysis. In the FEM-SO, the total CPU time is about 0.50 seconds, while that of direct FEM is about 20 seconds. The proposed method can greatly improve the computational efficiency for a long-period structure as compared with the conventional FEM. In addition, the analysis of a structure having a short interface region is highly efficient because the size of scattering operators is small. The computer memory used in this analysis is only 0.17GB for the FEM-SO, while it is 10GB for the direct FEM.

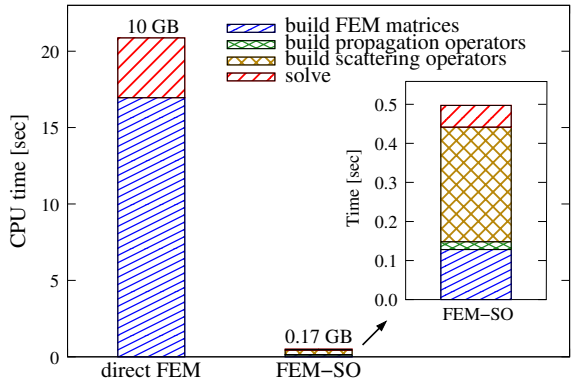

Fig. 11. CPU time and memory usage in each method for analysis of the problem shown in Fig. 8.

IV. CONCLUSION

A novel SO technique is presented with the help of FEM and implementation of POM boundary conditions. The presented FEM-SO has a great advantage not founded in other SO techniques, that is to say, arbitrary structure can be discretized by finite element meshes and divided into fundamental segments at arbitrary cross-sections. The boundary condition for connecting at discontinuity interface must be satisfied, and we introduced a special interface matrix. In two numerical simulation results, we showed the validity of the formulated scattering matrix and interface matrix, that includes excitation of various radiation modes and resonant operation caused by a periodic structure. This method is compatible with BiBPM [18]–[20], that is, by applying the FEM-SO to arbitrary structures and by applying the BiBPM to z-invariant structures, mesh-free sections can be configured. In addition, it has been confirmed that the propagation operator is useful even in plasmonics [36], and it seems that the proposed method can be readily extended to plasmonic waveguides. Since FEM-based propagation operators using line elements can be extended to 3-D vectorial operators by using conventional 2-D elements [26], it is promising to make 3-D FEM-SO combining the 3-D operators with conventional 3-D FEM [37]. With respect to waveguide design application, when iterative calculation with variation of a part of the structure is necessary (most of optical waveguide designs correspond to this), it is expected to greatly improve the efficiency by omitting the recalculation of the scattering operators of the invariant segments. Furthermore, different waveform incidence case and backward incidence case can be studied simultaneously with few additional computations. Thus, it is clear that the FEM-SO can be an efficient analysis method in various optical waveguide designs.

REFERENCES

[1] M. D. Feit and J. A. Fleck, "Light propagation in graded-index optical fibers," *Appl. Opt.*, vol. 17, no. 24, pp/ 3990-3998, Dec. 1978.
[2] W. P. Huang and C. L. Xu, "Simulation of three-dimensional optical waveguides by a full-vector beam propagation method," *IEEE J. Quantum Electron.*, vol. 29, no. 10, pp. 2639-2649, Oct. 1993.
[3] Y. Tsuji and M. Koshiba, "A finite element beam propagation method for strongly guiding and longitudinally varying optical waveguides," *J. Lightw. Technol.*, vol. 14, no. 2, pp. 217-222, Feb. 1996.
[4] Y. Tsuji and M. Koshiba, "Finite element beam propagation method for three-dimensional optical wveguide structures," *J. Lightw. Technol.*, vol. 15, no. 9, pp. 1728-1734, Sep. 1997.
[5] J. Yamauchi, G. Takahashi, and H. Nakano, "Full-vectorial beam-propagation method based on the McKee-Mitchell scheme with improved finite-difference formulas," *J. Lightw. Technol.*, vol. 16, no. 12, pp. 2458-2464, Dec. 1998.
[6] Y. Tsuji and M. Koshiba, "Adaptive mesh generation for full-vectorial guided-mode and beam-propagation solutions," *IEEE J. Sel. Topics Quantum Electron.*, vol. 6, no. 1, pp. 163-169, Jan. 2000.
[7] G. Sztefka and H. P. Nolting, "Bidirectional eigenmode propagation for large refractive index steps," *IEEE Photon. Technol. Lett.*, vol. 5, no. 5, May 1993.
[8] J. Willems, J. Haes, and R. Baets, "The bidirectional mode expansion method for two-dimensional waveguides: the TM case," *Opt. Quantum Electorn.*, vol. 27, no. 10, pp. 995-1007, Oct. 1995.
[9] M.-S. Kwon, "A numerical stable analysis method for complex multilayer waveguides based on modified transfer-matrix equations," *J. Lightw. Technol.*, vol. 27, no. 20, pp. 4407-4414, Oct. 2009.
[10] H. Liang, J. Mu, R. A. Soref, X. Li, and W. P. Huang, "An optical mode-matching method with improved accuracy and efficiency," *IEEE J. Quantum Electron.*, vol. 51, no. 2, #6100108, Feb. 2015.
[11] H. Rao, R. Scarmozzino, and M. Osgood, "A bidirectional beam propagation method for multiple dielectric interfaces," *IEEE photon. Technol. Lett.*, vol. 11, no. 7, Jul. 1999.
[12] H. E.-Refaei, D. Yevick, and I. Betty, "Stable and noniterative bidirectional beam propagation method," *IEEE Photon. Technol. Lett.*, vol. 12, no. 4, Apr. 2000.
[13] J. Xiao, S. Wu, and X. Sun, "A stable and accurate preconditioner for bidirectional beam propagation method," *IEEE J. Quantum Electron.*, vol. 51, no. 4, #6100107, Apr. 2015.
[14] K. Morimoto and Y. Tsuji, "Analysis of multiple waveguide discontinuities using propagation operator method and beam propagation method," *IEEE J. Quantum Electron.*, vol. 55, no. 4, #6100108, Aug. 2019.
[15] P. Bienstman and R. Baets, "Optical modelling of photonic crystals and VCSELs using eigenmode expansion and perfectly matched layers," *Opt. Quantum Electron.*, vol. 33, no. 4/5, pp. 327-341, Apr. 2001.
[16] J. Čtyroký, "A simple bi-directional mode expansion propagation algorithm based on modes of a parallel-plate waveguide," *Opt. Quantum Electron.*, vol. 38, pp. 45-62, 2006.
[17] J. Čtyroký, "Improved bidirectional-mode expansion propagation algorithm based on Fourier series," *J. Lightw. Technol.*, vol. 25, no. 9, pp. 2321-2330, Sep. 2007.
[18] P. L. Ho and Y. Y. Lu, "A stable bidirectional propagation method based on scattering operators," *IEEE Photon. Technol. Lett.*, vol. 13, no. 12, pp. 1316-1318, Dec. 2001.
[19] P. L. Ho and Y. Y. Lu, "A bidirectional beam propagation method for periodic waveguides," *IEEE Photon. Technol. Lett.*, vol. 14, no. 3, pp. 325-327, Mar. 2002.
[20] H. Zhang, J. Mu, and W.-P. Huang, "Improved bidirectional beam-propagation method by a fourth-order finite-difference scheme," *J. Lightw. Technol.*, vol. 25, no. 9, pp. 2807-2813, Sep. 2007.
[21] Z. Zhang, Y. Tsuji, T. Yasui, and M. Eguchi, "Design of ultra-compact triplexer with function-expansion based topology optimization," *Opt. Express*, vol. 23, no. 4, pp. 3936-3950, Feb. 2015.
[22] Z. Yu, H. Cui, and X. Sun, "Genetic-algorithm-optimized wideband on-chip polarization rotator with and ultrasmall footprint," *Opt. Lett.*, vol. 42, no. 16, pp. 3093-3096, Aug. 2017.
[23] A. Koda, K. Morimoto, and Y. Tsuji, "A study on topology optimization of plasmonic waveguide devices using function expansion method and evolutionary approach," *J. Lightw. Technol.*, vol. 37, no. 3, pp. 981-988, Feb. 2019.
[24] S. S. A. Obayya, "Novel finite element analysis of optical waveguide discontinuity problems," *J. Lightw. Technol.*, vol. 22, no. 5, pp. 1420-1425, May 2004.
[25] S. Wu and J. Xiao, "An efficient semivectorial bidirectional beam propagation method for 3-D optical waveguide structures," *J. Lightw. Technol.*, vol. 34, no. 4, pp. 1313-1321, Feb. 2016.
[26] K. Morimoto and Y. Tsuji, "Full-vectorial analysis of optical waveguide discontinuities using propagation operator method based on finite element method," *OSA Continuum*, vol. 2, no. 3, pp. 540-553, Mar. 2019.
[27] Y. Tsuji and M. Koshiba, "Finite element method using port truncation by perfectly matched layer boundary conditions for optical waveguide discontinuity problems," *J. Lightw. Technol.*, vol. 20, no. 3, pp. 463-468, Mar. 2002.
[28] M. Koshiba, "Optical waveguide theory by the finite element method," *IEICE Trans. Electron.*, vol. E97-C, no. 7, pp. 625-635, July 2014.

[29] K. Morimoto, A. Iguchi, and Y. Tsuji, "Propagation operator based boundary condition for finite element analysis," *IEEE Photon. J.*, vol. 12, no. 4, pp. #6601713, Aug. 2020.
[30] Y. S. Choi-Grogan, K. Eswar, P. Sadayappan, and R. Lee, "Sequential and parallel implementations of the partitioning finite-element method," *IEEE Trans. Antennas Propag.*, vol. 44, no. 12, pp. 1609-1616, Dec. 1996.
[31] J.-D. Benamou and B. Desprès, "A domain decomposition method for the Helmholtz equation and related optimal control problems," *J. Comput. Phys.*, vol. 136, pp. 68-82, 1997.
[32] S. Yoneta, M. Koshiba, and Y. Tsuji, "Combination of beam propagation method and finite element method for optical beam propagation analysis," *J. Lightw. Technol.*, vol. 17, no. 11, pp. 2398-2404, Nov. 1999.
[33] M. I. Davanço, C. E. R.-Mercedes, and H. E. H.-Figueroa, "Novel boundary condition for the finite-element solution of arbitrary planar junction," *IEEE Photon. Technol. Lett.*, vol. 13, pp. 46-47, 2001.
[34] C. E. R.-Mercedes and H. E. H.-Figueroa, "Padé boundary conditions for the finite-element modeling of arbitrary planar junctions," *J. Lightw. Technol.*, vol. 22, no. 2, pp. 669-676, Feb. 2004.
[35] L. Li, "Formulation and comparison of two recursive matrix algorithms for modeling layered diffraction gratings," *J. Opt. Soc. Am. A*, vol. 13, no. 5, pp. 1024-1035, May 1996.
[36] K. Morimoto and Y. Tsuji, "An efficient analysis of butt coupling between dielectric and plasmonic waveguide using propagation operator method based on finite element scheme," *JSST 2018 The 37th Annual International Conference on Simulation Technology*, Hokkaido, Japan, 2018.
[37] T. Yasui, Y. Tsuji, J. Sugisaka, and K. Hirayama, "Design of three-dimensional optical circuit devices by using topology optimization method with function-expansion-based refractive index distribution," *J, Lightw. Technol.*, vol. 31, no. 23, pp. 3765-3770, Dec. 2013.

Keita Morimoto received the B.S. and M.S. degrees in information and electronic engineering from Muroran Institute of Technology, Muroran, Japan, in 2017 and 2019, respectively, where he is currently pursuing the Ph.D. degree in information and electronic engineering.

Mr. Morimoto is a Student Member of the Institute of Electronics, Information and Communication Engineers (IEICE) and IEEE.

Akito Iguchi received the B.S., M.S., and Ph.D. degrees in electronic engineering from Muroran Institute of Technology, Muroran, Japan, in 2015 and 2017, and 2019. From 2019 to 2020, he was a Post-Doctoral Research Fellow of Japan Society for the Promotion of Science (JSPS). He is currently an Assistant Professor at Muroran Institute of Technology.

Dr. Iguchi is a member of the Institute of Electronics, Information and Communication Engineers (IEICE) and IEEE.

Yasuhide Tsuji (M'97) received the B.S., M.S., and Ph.D. degrees in electronic engineering from Hokkaido University, Sapporo, Japan, in 1991, 1993, and 1996, respectively.

In 1996, he joined the Department of Applied Electronic Engineering, Hokkaido Institute of Technology, Sapporo, Japan. From 1997 to 2004, he was an Associate Professor of Electronics and Information Engineering at Hokkaido University. From 2004 to 2011, he was an Associate Professor of Electrical and Electronic Engineering at Kitami Institute of Technology, Kitami, Japan. Since 2011, he has been a Professor of Information and Electronic Engineering at Muroran Institute of Technology, Muroran, Japan. He has been interested in wave electronics.

Dr. Tsuji is a Senior Member of the Institute of Electronics, Information and Communication Engineers (IEICE), IEEE, and the Optical Society of America (OSA), and a Member of the Japan Society of Applied Physics. In 1997, 1999, and 2019, he was awarded the Excellent Paper Award from IEICE. In 2000, he has received the Third Millennium Medal from IEEE. In 2019, he recieved the IEEE Photonics Technology Letters Outstanding Reviewer Award.